Journal of Applied Polymer Science

Cooling rate dependence of the crystallinity at nonisothermal crystallization of polymers: A phenomenological model

Jürgen E. K. Schawe
METTLER TOLEDO AG, Sonnenbergstrasse 74, Schwerzenbach 8603, Switzerland
Correspondence to: J. E. K. Schawe (E-mail:Juergen.Schawe@Mt.Com)

ABSTRACT: The cooling rate dependence of the crystallinity of polymers is investigated via the example of different technical polypropylenes using fast scanning calorimetry (FSC) in a cooling rate range between 1 and 5000 K s^{-1}. In the slower cooling rate range (below 100 K s^{-1}) the crystallinity increases slightly with decreasing cooling rate. Above cooling at 100 K s^{-1} the crystallinity decreases substantially and vanishes at the critical cooling rate. We describe this behavior using a simplified model with two components: the generic crystallinity function and the retardation function. For a mathematical description, we use empirically fitted functions that describe the cooling rate dependence of the crystallinity and the critical cooling rate. © 2015 Wiley Periodicals, Inc. J. Appl. Polym. Sci. **2016**, *133*, 42977.

KEYWORDS: crystallization; differential scanning calorimetry; kinetics

Received 28 July 2015; accepted 23 September 2015
DOI: 10.1002/app.42977

INTRODUCTION

Knowledge of the structure development of semicrystalline polymers during processing is important to understand the correlation between processing conditions and product behavior. An important parameter for the structural characterization of semicrystalline polymers is the crystallinity, α. Mechanical properties like shrinkage, impact behavior or stiffness, and optical properties are strongly influenced by the crystallinity.[1–3] The investigation and simulation of polymer crystallization during cooling is an ongoing task in polymer science and engineering.[4–10] The development has two basic directions, new and advanced methods for evaluation and description of the crystallization kinetics and the use of new experimental techniques.

In the last 15 years, several experimental techniques have been developed to study the polymer crystallization at processing-relevant cooling rates.[6,11–14] One of these techniques is the fast scanning calorimetry (FSC) based on chip sensors.[15–18] Nowadays, this technique is extensively used to study the crystallization and nucleation kinetics of polymers.[7,9,10,18–21]

For characterization, prediction and simulation of the crystallization kinetics, principally two different approaches are used: the isoconversional kinetics and the use of models of the crystallization kinetics. In the case of isoconversional kinetics, the effective activation energy as a function of the crystallinity is determined from measured curves.[21–23] This technique can be also used to determine characteristic parameters of crystallization models.[24]

Different approaches for modelling of the polymer crystallization exist.[5,7,8,25–28] In most of them, the temperature dependence of the crystallization rate is described by the standard model developed by Hoffman and Lauritzen (HL).[29] The kinetics of the growth process is usually described by the Kolmogorov–Johnson–Mehl–Avrami (KJMA) equation.[30–34] For the nonisothermal crystallization, different modifications of the KJMA equation,[35–40] or the Ozawa equation[40–42] are proposed.

For the determination of the final crystallinity after nonisothermal crystallization of polymers, all these theoretical and practice-driven approaches yield to numerical calculations based on large numbers of parameters. These parameters are determined by independent experiments or by fitting of experimental curves. In each model, predictions of the final crystallinity are problematic for conditions which are not similar to the experimental requirements of the parameter collection. In many cases, the kinetic analysis of nonisothermal crystallization processes is therefore a formal kinetic analysis and the evaluated parameters are often just fitted parameters with little to no physical meaning.

Polymers are semicrystalline materials and always contain amorphous fractions. This fact is often not incorporated in kinetic analyses and many approaches therefore do not consider the dependence of the final crystallinity on the experimental conditions. This means that the cooling rate dependence of the resulting crystallinity must be separately incorporated into such approaches. For this reason, we propose a numerically stable and mathematically easy approach to describe the final

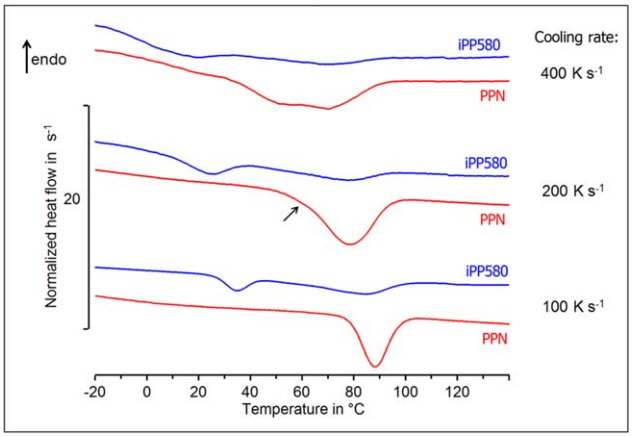

Figure 1. Selected cooling curves of the two PP materials. The arrow indicates a weak shoulder of the crystallization peak of PPN at cooling with 200 K s^{-1}. [Color figure can be viewed in the online issue, which is available at wileyonlinelibrary.com.]

crystallinity after a cooling process. We use a simple model function with a low number of fitting parameters to describe experimental data of the cooling rate dependence of the crystallinity over a wide range of cooling ratesa. The resulting data can easily be used for further calculations or for instance simulation of the structure formation during processing. Our approach to describe the crystallinity as a function of the cooling rate is illustrated via the example of polypropylene (PP).

EXPERIMENTAL

Samples

Two different, commercially available, types of polypropylene (PP) with different kinetic behaviors are used. iPP580 is an isotactic polypropylene purchased from Aldrich (427853, batch# 15619MD) with molecular masses of M_n = 166 kg mol^{-1} and M_w = 580 kg mol^{-1}. The melt flow index (MFI) determined for 2.16 kg at 230°C is 0.05 g $(10\ min)^{-1}$. An extensive thermal characterization of the crystallization and melting behavior is given in Ref. 20. The other material is PPN (Novolen 1106H from Basell) with M_n = 85 kg mol^{-1}, M_w = 462 kg mol^{-1}, and MFI = 2.0 g $(10\ min)^{-1}$. This material was selected because it shows an unusual crystallization behavior. In the temperature range below 80°C a second, α-phase, crystallization process was observed for this material.[43]

Measuring Instrument

For the FSC measurements the chip calorimeter from METTLER TOLEDO (Flash DSC 1 with UFS1 sensors) was used. The Flash DSC 1 was connected to an IntraCooler. Nitrogen (80 mL min^{-1}) was used as purge gas. For the measurements the temperature of the sensor support was set to be −90°C. The Flash DSC 1 is described in detail in Refs. 17, 18.

The Flash DSC measurements were performed on samples with a typical mass of about 50 ng. To prepare such samples, a part of the granulate piece was fixed in a razor blade microtome and approximately 10 μm thin slices were made. With the help of a microscope and a scalpel the film was cut into small parts with a characteristic edge length of 50 μm. Using a hair with a native tip the sample was carried and placed on the sample side of the UFS1 sensor. Afterwards, the samples were heated to above their melting temperature to ensure good thermal contact. If the sample formed a meniscus after heating, it was smeared on to the sensor using a thin copper wire. The sample thickness was estimated to be about 5 μm.

RESULTS

Flash DSC cooling measurements from 200 to −60°C were performed at various constant cooling rates between 1 and 5000 K s^{-1}. After each cooling segment the samples were heated with 1000 K s^{-1} to measure the melting and reorganization behavior. A selection of cooling curves is shown in Figure 1. iPP580 shows two crystallization peaks for cooling rates faster than 50 K s^{-1}. The low temperature process is usually discussed as the mesophase crystallization and the high temperature process is caused by α-phase formation.[18] PPN behaves differently: the low temperature peak occurs at a significantly higher temperature. In this case the behavior is interpreted as the consequence of two differently nucleated crystallization processes of α-phase.[43]

The temperatures of the peak and shoulders from the measured curves (Figure 1) are plotted in Figure 2 as a function of the cooling rate, β. The high temperature crystallization process of both materials is similar (crystallization of the α-phase). However, the figure clearly indicates the faster crystallization of PPN compared to iPP580. Larger differences occur in the low temperature process. While iPP580 forms the mesomorphous phase below 40°C at fast cooling rates,[18] PPN crystallizes to a differently nucleated α-phase below 60°C.[43]

The samples are first cooled at rates between 1 and 5000 K s^{-1}. Subsequently there are heated with 1000 K s^{-1}. A selection of heating curves is plotted in Figure 3. The curves are labeled with the rate of the previous cooling segment. After slow cooling rates, the heating curves only show a broad glass transition

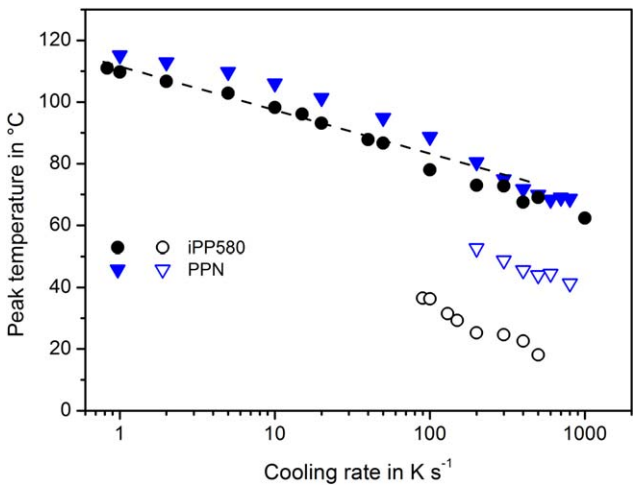

Figure 2. Peak temperatures of the crystallization peaks as a function of the cooling rate. The data point at 200 K s^{-1} of the low temperature crystallization of PPN was taken from a shoulder of the peak (see Figure 1). [Color figure can be viewed in the online issue, which is available at wileyonlinelibrary.com.]

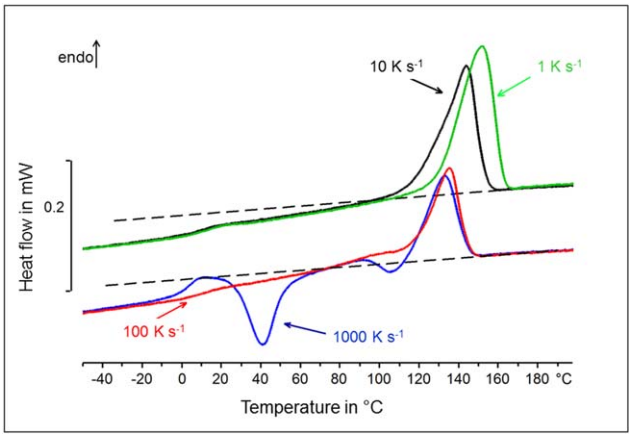

Figure 3. Selected heating curves of iPP580 measured at 1000 K s^{-1} after cooling at different rates. The dashed lines represent the extrapolations from the melt behavior. [Color figure can be viewed in the online issue, which is available at wileyonlinelibrary.com.]

at about 10°C and a final melting peak. After cooling at faster rates (100 K s^{-1}) the samples show reorganization during heating before the melting peak. The samples cooled faster as 100 K s^{-1} have a reduced crystallinity. This is indicated by the cold crystallization peak after the glass transition and the subsequent reorganization events. The heating curves of iPP580 and PPN are similar.

The crystallinity after the cooling process, α_c, is proportional to the specific crystallization enthalpy, Δh, determined from the cooling curves or the specific melting enthalpy evaluated from the subsequent heating curves. Since the relative experimental errors from the evaluation of the crystallization peaks are larger, the heating curves are taken for the evaluation. Because of the unknown sample mass, m, the enthalpy of melting, $\Delta H = m\,\Delta h$, was determined by peak evaluation. The extrapolation from the melt (dashed lines in Figure 3) was taken as the baseline for the evaluation. For the almost amorphous material, the integration limits reach from just above the glass transition (ca. 15°C) to the melt (ca. 160°C). From the melting enthalpy, we can determine the relative crystallinity, α_r,

$$\alpha_r = \frac{\alpha_c}{\alpha_{\mathrm{ref}}} = \frac{\Delta H}{\Delta H_{\mathrm{ref}}} \tag{1}$$

where α_{ref} is the crystallinity at a reference cooling rate and ΔH_{ref} is the related enthalpy. We select 1 K s^{-1} as the reference cooling rate. Figure 4 shows the measured cooling rate dependence of α_r.

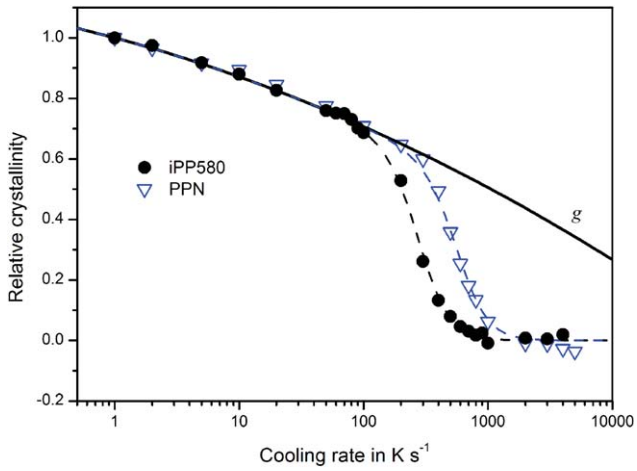

Figure 4. Relative crystallinity as a function of cooling rate for iPP580 and PPN. The solid curve represents the generic crystallinity function $g(\beta)$. The dashed curves are the fitted functions according to eq. (3). [Color figure can be viewed in the online issue, which is available at wileyonlinelibrary.com.]

At relatively slow cooling the crystallinity decreases slightly with increasing cooling rates. However, a further increasing (faster 100 K s^{-1}) of the cooling rate yields to a step-like decrease of crystallinity until the material becomes amorphous at about 1000 K s^{-1}. A similar dependence of the crystallinity on the cooling rates was reported for several polymers.[6,10]

DISCUSSION

The standard model for the temperature dependence of the crystallization process is based on the Turnbull–Fisher theory[44,45]:

$$\frac{1}{r_c} \propto t_{1/2} \propto \exp\left(\frac{U+\Delta G}{RT}\right) \tag{2}$$

where r_c is the crystallization rate, $t_{1/2}$ is the crystallization half time, U is the activation energy for the molecular transport to the crystal growth face, ΔG is the activation barrier for the nucleation processes, and R is the gas constant.

This theory describes the temperature dependence of the crystallization half time by two factors: the thermodynamically determined factor (exp $\Delta G/RT$) increases with temperature increase and the mobility determined factor (exp U/RT) decreases with temperature increase.

The typical behavior of the crystallization half time, $t_{1/2}$, is drawn in Figure 5. At high temperatures, the thermodynamic factor dominates the crystallization process. This means that the nucleation processes (primary and secondary nucleation) basically control the crystallization process. At lower temperatures, the crystallization half time increases with decreasing crystallization temperature. In this region, the mobility factor dominates the crystallization process: the crystallization is mainly controlled by the molecular transport to the crystal growth face. The inserted diagram shows a typical, isothermal crystallization curve. The peak maximum time is in good approximation identical to $t_{1/2}$. The onset and endset of the isothermal crystallization process are symbolized by the related curves t_{on} and t_{end}. The main crystallization process occurs between these limiting lines. The dash-dot lines in Figure 5 represent the cooling processes (at constant rates). The cooling rates increase from curves 1 to 8. We will use this simplified model to describe the measured behavior in Figure 4.

The behavior at cooling rates below 100 K s^{-1} is characterized by curves 1–4 in Figure 5. In this range, the curves cross the t_{on} and t_{end} curves. This means that the main crystallization process is basically finished and the temperature dependence of the

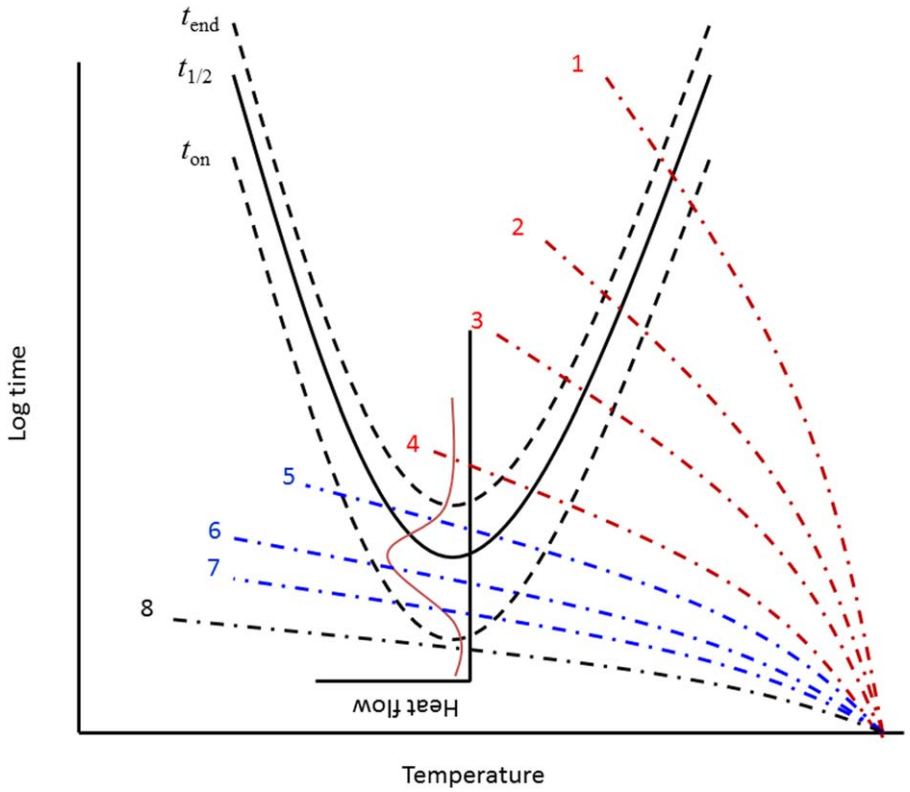

Figure 5. Schematic drawing of the temperature dependence of the crystallization process. $t_{1/2}$ is the crystallization half time as a function of the temperature. The heat flow curve of the isothermal crystallization process is displaced in the insert. The temperature dependencies of the onset and the endset are represented by the curves t_{on} and t_{end}. The temperature behavior of cooling experiments at constant cooling rates is symbolized by the dash-dot lines 1–8. [Color figure can be viewed in the online issue, which is available at wileyonlinelibrary.com.]

crystallization rate is largely determined by the thermodynamic factor. We call this range generic crystallization. For the materials of investigation the cooling rate dependence in this region (at slow cooling rates) is identical in good approximation.

The total cooling rate dependent crystallization process additionally contains significant material dependent s-type decay. From this figure, we deduce a simple phenomenological description of the cooling rate dependent crystallinity according to

$$\alpha_r = \frac{\alpha}{\alpha_{ref}} = g(\log\beta)\, v(\log\beta) \qquad (3)$$

where g is the generic crystallinity function and v is the retardation function.

The retardation function, v, describes the reduction of crystallinity at faster cooling rates for which the endset curve is not crossed. This behavior is significantly influenced by the diffusion factor of the TF theory. In Figure 5, this range is indicated by the cooling lines 5–7.

The retardation function v is 1 in the generic crystallization range (lines 1–4) and 0 if the material does not crystallize (dash-dot line 8). The related cooling rate is the so-called critical cooling rate, β_c. This is the slowest cooling rate at which no crystallization occurs and the material becomes an amorphous glass below the glass transition temperature.

Principally, the generic crystallization function can be described using crystallization models with multiple parameters.[7,26] We suggest fitting of the experimental data in the relevant cooling rate range with a practicable function containing a minimum

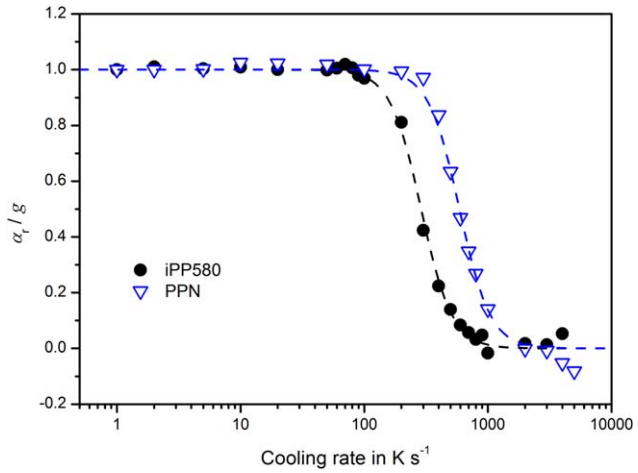

Figure 6. Retardation function values for both materials versus cooling rate. The dashed curves are fit results. [Color figure can be viewed in the online issue, which is available at wileyonlinelibrary.com.]

number of parameters. In the present case we use a simple quadratic function:

$$g(\log\beta) = 1 - a_1 \log(\beta) - a_2 (\log(\beta))^2 \quad (4)$$

The cooling rate has the unit K s^{-1}. We present arguments for the selection of this equation in the appendix. The two parameters (a_1 = 0.11, a_2 = 0.018) are determined by fitting the experimental data of both materials from Figure 4 in the cooling rate range from 1 to 100 K s^{-1}. The function is plotted in Figure 4. This behavior appears to be similar for all PP.

For the determination of the retardation function, the measured relative crystallinity is divided by the generic crystallization function (Figure 6).The resulting step-function can be fitted by

$$v(\log\beta) = (1+\exp(k\log(\beta/\beta_0))^{-1} \quad (5)$$

The parameter k describes the width of the step. Increasing k decreases the width of the step. The characteristic cooling rate, β_0, is the rate at the half step-height of v and thus describes the step position.

The data of both materials in Figure 6 can be fitted with the same width parameter of k = 8. The characteristic cooling rate was determined to be β_0 = 288 K s^{-1} for iPP580 and β_0 = 588 K s^{-1} for PPN. The fitting functions are displayed in Figure 6.

By combining the functions g and v according to eq. (3), the total curve of the cooling rate dependent crystallinity curve can be described (dashed curves in Figure 4).

The retardation function can also be used to estimate the critical cooling rate. From eq. (5) follows that the $1/p$ part of the step height is reached at

$$\log\beta_n = \frac{\ln(p-1)}{k} + \log(\beta_0) \quad (6)$$

If we assume that no crystallization occurs at cooling rates for which the retardation function v reaches the small value of 0.01, the critical cooling rate, β_c, can be calculated from

$$\log\beta_c \cong \frac{4.6}{k} + \log(\beta_0) \quad (7)$$

For the investigated materials then follows a critical cooling rate of 1100 K s^{-1} for iPP580 and 2200 K s^{-1} for PPN. This is in agreement with the experimental results.

CONCLUSIONS

Using flash DSC, the cooling rate dependent crystallization process can be studied over several orders of magnitude. In this study more than 3.5 decades (1–5000 K s^{-1}) are used to measure crystallization behavior. As a result, the cooling rate dependence of the crystallization temperature and the crystallinity can be measured. The cooling rate dependence of the crystallinity is an important parameter for understanding the material behavior after processing and to optimize processing conditions.

For a formal description of the experimental results, we introduce two functions: the generic crystallization function and the retardation function. For the investigated PP materials with different crystallization behavior the generic crystallization function is identical.

The decrease of crystallinity at faster cooling rates is described by a reduction function. This is a function with two parameters. The width-parameter can be taken as constant for the investigated materials. The characteristic cooling rate is material dependent. The approach presented here can be used to estimate the critical cooling rate at which materials do not crystallize during cooling.

The proposed equation can be used as an expansion of nonisothermal kinetic approaches and for numerical simulation of the structural formation at processing. Furthermore, this equation is applicable for quantification of differences in the crystallization behavior at fast cooling rate for different materials or influences of additives.

APPENDIX

For the polymer crystallization, the course of the crystallinity as a function of temperature and time is usually described by

$$\alpha(t,T) = \alpha_s(t,T) \cdot X(t,T) \quad (A1)$$

where α_s and X describe the kinetics of the secondary as well as the primary crystallization.

The function $X(t, T)$ can be expressed by the (KJMA) equation:[30–34]

$$X(t,T) = (1-\exp(-k_{\mathrm{KJMA}}(T)\, t^n)) \quad (A2)$$

where k_{KJMA} and n are the Avrami parameters. Reference (29) proposes a logarithmic equation to describe the kinetics of the lamella thickening after the primary crystallization. We extend this to the total secondary crystallization:

$$\alpha_s(t,T) = B(T)\log t \quad (A3)$$

We now estimate the maximum crystallinity of the cooling process below the glass transition temperature T_g. The primary crystallization process is finished at the endset temperature of the crystallization peak, T_2 (with $T_2 \gg T_g$). At T_2, we can set $X(T)$ = 1 and the increase of the crystallinity is caused by the secondary crystallization, which is described by eq. (A3).

To a first approximation we assume a linear function for the temperature-dependent factor B in eq. (A3)

$$B(T) = \begin{cases} b(T - T_{\min}) & \text{for } T \geq T_{\min} \\ 0 & \text{for } T < T_{\min} \end{cases} \quad (A4)$$

At temperatures below the minimum temperature, $T_{\min}$, the material does not show secondary crystallization.

The temperature dependence of α_s can be approximate by

$$\alpha_s = \frac{1}{\beta}\int_{T_1}^{T} \frac{d\alpha_s}{dt}\, dT \quad (A5)$$

For the determination of the maximum crystallinity at a certain cooling rate the integration limits are T_1 and T_2, these are the onset and endset temperatures of the crystallization peak during cooling.

By inserting of

$$T = T_f - \beta t \tag{A6}$$

(T_f is the temperature of fusion) in eq. (A4), we get the time derivative of α_s:

$$\frac{d\alpha_s}{dt} = b\beta\left(\frac{T_f - T_{\min}}{\beta t} - 1 - \log t\right) \tag{A7}$$

By substitution of $t = (T_f - T)/\beta$ in eq. (A7), we get the maximum crystallinity at cooling with β form the solution of eq. (A5):

$$\alpha(\beta) = b\left((T_f - T_{\min})\log\left(\frac{T_f - T_1}{T_f - T_2}\right) + (T_f - T_2)\log\left(\frac{T_f - T_2}{\beta}\right) - (T_f - T_1)\log\left(\frac{T_f - T_1}{\beta}\right)\right) \tag{A8}$$

The cooling rate dependence of the peak temperature of the crystallization peak can be estimated from the results in Figure 2 (dashed line) to be

$$T_{\text{peak}}(\beta) = T_{\text{peak},0} - \tau \log\beta \tag{A9}$$

where $T_{\text{peak},0} = T_{\text{peak}}(\beta = 1\ \text{K s}^{-1})$. The slope τ is nearly constant. The same approach can be taken for the onset and the endset:

$$T_1(\beta) = T_{1,0} - \tau_1 \log\beta \tag{A10}$$

$$T_2(\beta) = T_{2,0} - \tau_2 \log\beta \tag{A11}$$

Because the slope $\frac{d\log(T_f - T_i)}{d\log\beta}$ is about 0.1, we set $\log(T_f - T_i) \approx d_i$ to approximately cooling rate independent ($i = 1,2$). By inserting of eq. (A10) and (A11) in (A8) and arithmetic rearrangements follows:

$$\alpha(\beta) = c_0 - c_1 \log\beta - c_2 (\log\beta)^2 \tag{A12}$$

with the coefficients $c_0 = b\left((T_f - T_{\min})(d_1 - d_2) + d_2(T_f - T_{2,0}) - d_1(T_f - T_{1,0})\right)$, $c_1 = b(d_2\tau_2 - d_1\tau_1)$, and $c_2 = b(\tau_1 - \tau_2)$. This means that the existence of the quadratic term in eq. (A12) is mainly caused by the broadening of the crystallization peak with increasing the cooling rate.

For the coefficients in eq. (4), it now follows $a_1 = \frac{c_1}{c_0}\alpha_{\text{ref}}$ and $a_2 = \frac{c_2}{c_0}\alpha_{\text{ref}}$.

REFERENCES

1. Nielsen, L. E.; Landel, R. F. Mechanical Properties of Polymers and Composites; Marcel Dekker: New York, **1994**.
2. Mark, J.; Ngai, K; Graessley, W.; Mandelkern, L.; Samulski, E.; Koenig, J.; Wihnall, G. Physical Properties of Polymers; Cambridge University Press: Cambridge, **2003**.
3. Gedde, U. W. Polymer Physics; Kluwer Academic Publishers: Dordrecht, **1995**.
4. Janeschitz-Kriegl, H. Crystallization Modalities in Polymer Melt Processing; Springer: Wien, **2010**.
5. Di Laurenzo, M. L.; Silvestre, C. *Prog. Polym. Sci.* **1999**, *24*, 917.
6. Brucato, V.; Piccarolo, S.; La Carrubba, V. *Chem. Eng. Sci.* **2002**, *57*, 4129.
7. van Drongelen, M.; van Erp, T. B.; Peters, G. W. M. *Polymer* **2012**, *53*, 4758.
8. Liu, Z. J.; Quyang, J.; Zhou, W.; Wang, X. D. *Comput. Mat. Sci.* **2015**, *97*, 245.
9. Luijsterburg, B. J.; de Kort, G. W.; van Drongelen, M.; Govaert, L. E.; Goossens, J. G. P. *Thermochim. Acta* **2015**, *603*, 94.
10. Rhoades, A. M.; Williams, J. L.; Androsch, R. *Thermochim. Acta* **2015**, *603*, 103.
11. De Snatis, F.; Lamberti, G.; Peters, G. W. M.; Brucato, V. *Euro. Polym. J.* **2005**, *41*, 2297.
12. Nishida, K.; Okada, K.; Asakawa, H.; Matsuba, G.; Ito, K.; Kanaya, T.; Kaji, K. *Polym. J.* **2012**, *44*, 95.
13. van Drongelen, M.; Meijer-Vissers, T.; Cavallo, D.; Portale, G.; Vanden Poel, G.; Androsch, R. *Thermochim. Acta* **2013**, *563*, 33.
14. Stolte, I.; Cavallo, D.; Alfonso, G. C.; Portale, G.; van Drongelen, M.; Androsch, R. *Eur. Polym. J.* **2014**, *60*, 22.
15. Adamovsky, S. A.; Minakov, A. A.; Schick, C. *Thermochim. Acta* **2003**, *403*, 55.
16. Zhuravlev, E.; Schick, C. *Thermochim. Acta* **2010**, *505*, 14.
17. Mathot, V.; Pyda, M.; Pijpers, T.; Van den Poel, G.; van de Kerkhof, E.; van Herwaarden, S.; van Herwaarden, F.; Leenaers, A. *Thermochim. Acta* **2011**, *522*, 36.
18. Schawe, J. E. K. *J Therm. Anal. Calorim.* **2014**, *116*, 1165.
19. Androsch, R.; Rhoades, A. M.; Stolte, I.; Schick, C. *Euro. Polym. J.* **2015**, *66*, 180.
20. Schawe, J. E. K. *Thermochim. Acta* **2015**, *603*, 85.
21. Bosq, N.; Guigo, N.; Zhuravlev, E.; Sbirrazzuoli, N. *J. Phys. Chem. B* **2013**, *117*, 3407.
22. Kissinger, H. E. *Anal. Chem.* **1957**, *29*, 1702.
23. Orava, J.; Greer, A. L. *Thermochim. Acta* **2015**, *603*, 63.
24. Vyazovkin, S.; Sbirrazzuoli, N. *Macromol. Rapid Commun.* **2004**, *25*, 733.
25. Haudin, J. M.; Chenot, J. L. *Intern. Polym. Process.* **2004**, *14*, 267.
26. Dietz, W. *Colloids Polym. Sci.* **1981**, *259*, 413.
27. Coccorullo, I.; Pantani, R.; Titomanlio, G. *Polymer* **2003**, *44*, 307.
28. Piorkowska, E.; Galeski, A.; Haudin, J. M. *Prog. Polym. Sci.* **2006**, *31*, 549.
29. Hoffman, J. D.; Davis, G. T.; Lauritzen, J. I. Jr. in Treatise on Solid State Chemistry, Vol. 3; Hannay, N.B, Ed.; Plenium Press: New York, **1976**, p 497.
30. Avrami, M. *J Chem. Phys.* **1939**, *77*, 1103.
31. Avrami, M. *J Chem. Phys.* **1940**, *8*, 212.
32. Avrami, M. *J Chem. Phys.* **1941**, *9*, 177.
33. Kolmogorov, A. N. *Izvestiya Akad. Nauk SSSR Ser. Math.* **1937**, *1*, 355.
34. Johnson, W. A.; Mehl, R. F. *Trans. Am. Inst. Min. Engin.* **1939**, *135*, 416.
35. Woldt, E. *J. Phys. Chem. Solids* **1992**, *53*, 521.

36. Málek, J. *Thermochim. Acta* **1995**, *267*, 61.
37. Jeziorny, A. *Polymer* **1978**, *19*, 1142.
38. Mubarak, Y.; Harkin-Jones, E. M. A.; Martin, P. J.; Ahmad, M. *Polymer* **2001**, *42*, 3171.
39. Nakamura, K.; Watanabe, T.; Katayama, K.; Amano, T. *J. Appl. Polym. Sci.* **1972**, *16*, 1077.
40. Lambrigger, M. *Polym. Eng. Sci.* **2004**, *44*, 2194.
41. Ozawa, T. *Polymer* **1971**, *12*, 149.
42. Ozawa, T. *J. Therm. Anal.* **1976**, *9*, 369.
43. Schawe, J. E. K.; Vermeulen, P. A.; van Drongelen, M. *Thermochim. Acta* **2015**, *616*, 87.
44. Turnbull, D.; Fisher, J. C. *J. Chem. Phys.* **1949**, *17*, 71.
45. Sawada, K.; Ishida, Y. *J. Polym. Sci. Polym. Phys. Ed.* **1975**, *13*, 2247.